12th International Symposium on Turbulence and Shear Flow Phenomena (TSFP12)
Osaka, Japan, July 19–22, 2022

ANALYSIS OF LARGE-SCALE/SMALL-SCALE INTERACTIONS IN TURBULENT CHANNEL FLOW AT $RE_\tau = 5200$ USING AUTO-ENCODER COMBINED WITH MULTIVARIATE-PDF.

Agostini Lionel
Institut Pprime, CNRS / Université de Poitiers / ENSMA,
Poitiers, France
lionel.agostini@univ-poitiers.fr

Leschziner Michael
Department of Aeronautics,
Imperial College London,
London, UK

Cordier Laurent
Institut Pprime, CNRS / Université de Poitiers / ENSMA,
Poitiers, France

ABSTRACT

The influence of especially energetic structures residing in the region around $y^+ \approx 4.\sqrt{Re_\tau}$, are investigated in channel flow at $Re_\tau \approx 5200$. The motivation is to shed light on how the magnitude and length-scale properties of the small-scale near-wall turbulence are modulated by the outer structures, and whether this response is tied solely to the friction velocity – i.e., whether the near-wall turbulence is universal when scaled by the spatially and temporally varying large-scale wall shear stress, rather than by its time-averaged value. A unique aspect of the present framework is the use of an auto-encoder algorithm to separate the extremely large full-volume DNS fields into large-scale and small-scale motions. A second original element is a formalism that derives the modulation, conditional on large-scale fluctuations, from continuous statistical quantities represented as joint-multivariable probability-density functions, thus obviating the need for any discrete representation or binning beyond that imposed by the discrete DNS solution. A third novel aspect is the use of the length-scale-wise derivative of the second-order structure function to quantify the modulation (increase or decrease) in the length scale, again conditional on the large-scale structures.

1 Introduction

The impact of outer turbulent structures on the state of the viscosity-affected near-wall layer is of considerable interest in the context of controlling wall friction. The key aspects of this interaction are, first, the formation of large-scale fluctuations in the viscous and buffer layers, provoked by "footprinting" of outer scales in the log layer, and second, the attenuation or amplifications ("modulation") of small-scale motions in this layer by the footprints. Importantly, both effects rise with the Reynolds number, in tandem with the progressive rise in the streamwise turbulence energy around the location $y^+ \approx 4.\sqrt{Re_\tau}$ – i.e. $y^+ \approx 280$ at $Re_\tau = 5200$, the value considered herein. Thus, as Re rises, the near-wall layer is increasingly perturbed by the strengthening footprints, which is likely to increasingly compromise the effectiveness of any control method designed to reduce the friction drag by damping the small-scale turbulence in the viscosity-affected near-wall layer.

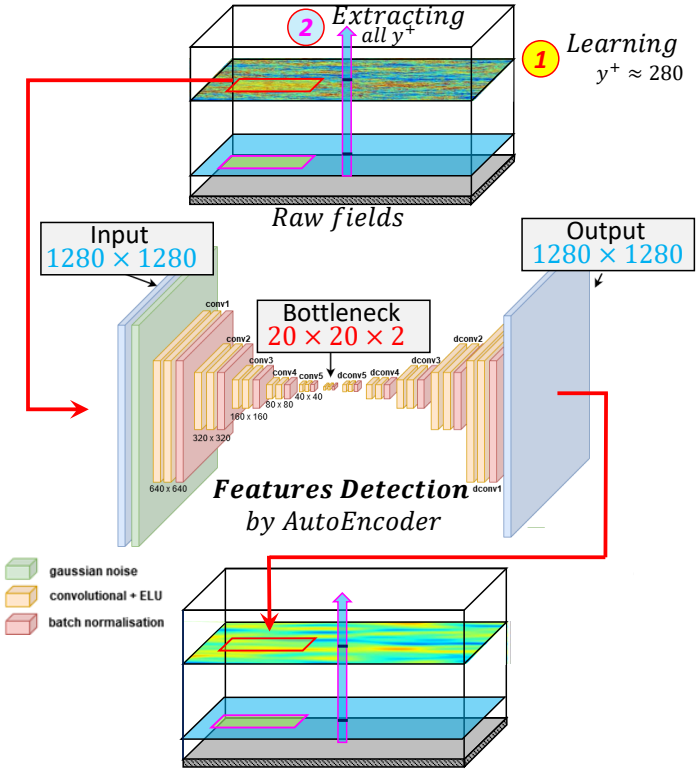

Figure 1. Schematic representation of the process of extracting the large-scale motions by using a multi-layer Auto-Encoder. Patches on the plane $y^+ \approx 280$ are subdomains of size $\Delta x^+ = 1280$, $\Delta z^+ = 1280$ used for the learning process.

Agostini & Leschziner (2014, 2019*a*,*b*) have previously examined a variety of aspects of the above large-scale/small-scale interactions by analysing the DNS data of Touber & Leschziner (2012) and Agostini & Leschziner (2014) for channel flow at $Re_\tau = 1000$, a value for which the interactions are relatively weak. They did so by employing their own spatially bi-dimensional "Empirical Mode Decomposition (Bi-EMD)" to separate the turbulence spectrum across many full-

volume DNS realisations into small, medium and large-scale modes and then constructing small-scale statistics, conditional on large-scale skin-friction footprints to infer the mechanisms by which small-scale amplification by positive footprints dominate asymmetrically over small-scale attenuation by negative footprints, thus explaining the progressive rise in the damaging perturbations of the near-wall layer by footprinting.

Although the statistical tools developed in previous studies can be applied, in principles, to data at higher Reynolds numbers, the resource requirements posed by the EMD quickly become untenable as the spectrum of scales, and thereby the size of the domain, widen rapidly with the Reynolds number. This all but prevents the application of the EMD to full-volume DNS data sets at $Re_\tau = 5200$, taken from Lee & Moser (2015). To circumvent this problem, a novel approach is proposed herein and analysed in this study in which a decoder-encoder deep-learning algorithm is used to separate the scales across any 2d $(x-z)$ plane into small-scale and large-scale fields. Once this is achieved, joint PDFs are constructed, as explained below, which allow the effects of the large-scale footprints on the small-scale near-wall layer to be studied.

The present paper deals with four aspects :

i the manner in which the decoder-encoder model is used to separate the scales over full-volume DNS realisations;
ii the type of conditional small-scale statistics derived from the separated fields.
iii the manner in which the statistics under (ii) yield insight into the mechanisms by which the large scales affect the small scales;
iv the manner in which the decomposition under (i) allows the "quasi-steady" hypothesis to be tested – -i.e. the proposition that the small-scale fields are universal when scaled with the instantaneous and local large-scale wall shear stress.

2 Methodology

2.1 Decoder-encoder-based scale separation

As noted earlier, the EMD becomes untenable at the present Reynolds number, to which must be added some limitations regarding the possibly incomplete capture of large-scale motions the size of which is comparable with the computational box size. Thus, an alternative data-driven methodology, referred to as "Auto-Encoder" (AE), has been adopted herein to separate the large-scale from small-scale motions. An AE is an unsupervised machine-learning (ML) algorithm that is trained to reconstruct a representation of its inputs from a data set that is highly reduced in volume and detail relative to the full input (Agostini, 2020). As illustrated in Fig.1, an AE has three parts: an encoder, a bottleneck (latent space), and a decoder. Depending on how its architecture is defined, an AE can served different purposes, functioning as de-noisors (Vincent *et al.*, 2010), anomaly detectors (Zhou & Paffenroth, 2017), and estimators (Guastoni *et al.*, 2021), for example. In the present study, the goal is to use AE for extracting large-scale motions associated to the outer-flow structure at any wall-normal location. By reducing the amount of information passing through the AE's bottleneck, the AE must learn the most significant features of the input so that the output image is as close as possible to the input image. The level of closeness is defined by the mean square of the reconstruction error (MSE), steering the AE towards reconstructing the most energetic scales. Once the training (learning) is achieved – here done by feeding in sub-domains of size 1280×1280 wall units, each being $1/48^{th}$ of the total data items in the plane, chosen randomly from 2D fields at $y^+ \approx 280$, where most energetic eddies correspond to large-scale motions – the AE will only use the "library" of features learned at this wall-normal location for extracting large-scale fluctuations produced by the outer-flow structures at any other wall-normal location. For the training, subsets from seven DNS snapshots are used, and for validation subsets from three other snapshots are used. A validation set is required to ensure that the features learned by the AE correspond to a valid statistical description of the external-flow structures. This means that not only the noise will be filtered out, but that also any singular events produced by the structures are removed, which is a distinctive benefit of the AE over other methods such as FFT- or EMD-based methodologies. The main advantage is that the AE, once trained, is able to identify information reflecting the true impact of external flow structures at any wall-normal location, and extract them faithfully in isolation from spurious disturbances having spectral length-scale features similar to the true LS structures, which is not possible with low-pass filtering, wherein all information of a given length-scale spectrum is conserved whatever its source.

The success of this process is illustrated in Figs.2 and 3, which show fields decomposition, spectra and streamwise energy profiles for the large-scale and small-scale motions respectively. Fig. 2 shows sub-domains of streamwise-fluctuations fields across the wall-normal plane $y^+ \approx 280$ and $y^+ \approx 12$ covering the sub-domain $x^+ \times z^+ \approx 16000 \times 8000$, corresponding to $1/8$ and $1/6$ of the total computational-box dimensions, respectively. Full streamwise-fluctuations fields at wall-normal locations $y^+ \approx 280$ and $y^+ \approx 12$ are conveyed by Figs.2(a) and 2(b), respectively. The large-scale motions and the residual small-scale fields at $y^+ \approx 12$ are shown in Figs. 2(c) and 2(d). Specific feature that deserve to be underlined are, first, the strong dominance of the large-scale component at the outer location; second, the presence of large-scale footprints in the near-wall layer; third, the fine-grained small-scale features in the near-wall layer; and fourth the influence of the large-scale footprints on the intensity of the small-scale structures in the near-wall layer.

Fig.3(a) demonstrates the scale-separation process by way of pre-multiplied energy-density spectra, in the $y^+ - \lambda_z^+$ (spanwise wavelength) plane for the streamwise components. The red contours identify the large scales, while the blue contours pertain to the small scales, the sum of the two being identified by the black contours. The corresponding energy profiles in the wall-normal direction are given on the right-hand-side (r.h.s) plots. The l.h.s plot convey a well-defined scale separation, with the large scales confined to wavelength values $\lambda_z^+ > 800$, which compares to $\lambda_z^+ \approx 100$ at which the streamwise energy density peaks at $y^+ \approx 12$.

2.2 Conditional analysis of amplitude modulation based on multivariate PDFs

In recent papers (Agostini & Leschziner (2019*a*,*b*, 2021)), a novel approach to analysing any statistical flow property conditional on any value of the large-scale skin-friction fluctuation is presented, bringing into focus the response of the turbulent statistics to the large-scale motions. Thus, with the large-scale/small-scale decomposition effected, conditional joint PDFs of the form $P(u_1,u_2,u_3,Cf_{LS})$ are derived from the DNS data, where Cf_{LS} is the "conditional variable" and u_1,u_2,u_3 are velocity fluctuations in the x,y,z directions, respectively. Conditional variables can then be extracted as exemplified by the following expressions for the mean velocity and Reynolds

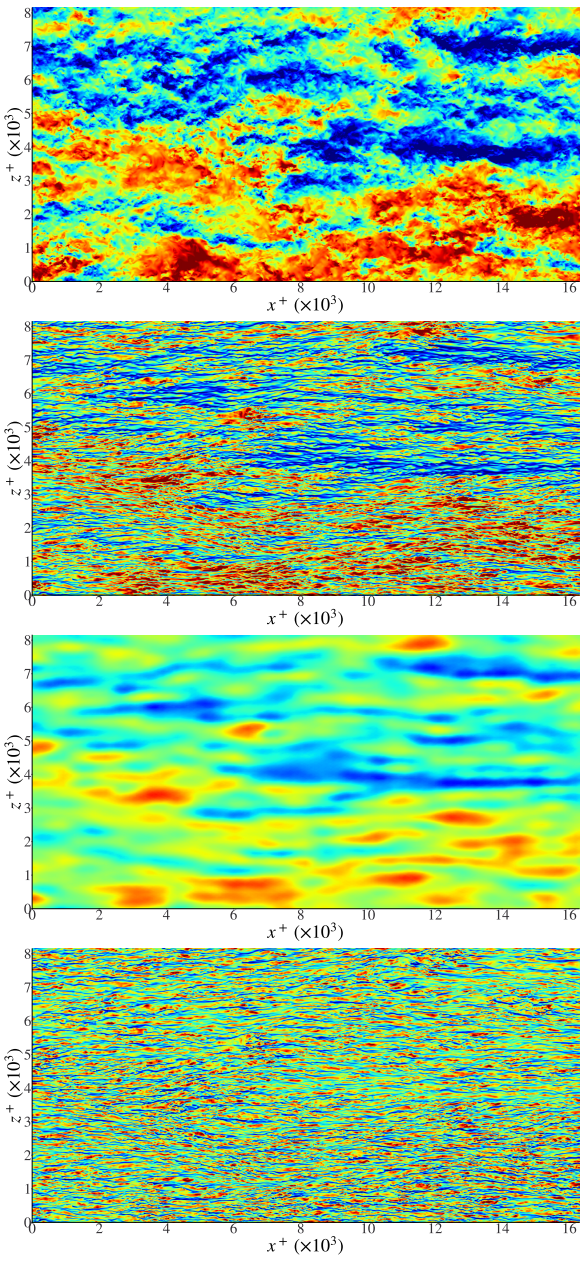

Figure 2. Illustration of scale decomposition using the approach shown in Fig. 1 at over a portion of the $x-z$ DNS box (1/8th in streamwise direction and 1/6th in streamwise direction); (a) and (b) full streamwise-fluctuations fields at $y^+ \approx 280$ and $y^+ \approx 13$, respectively; (c) large-scale fluctuations fields (output of the auto-encoder) at $y^+ \approx 13$ and (d) small-scale fluctuations (total minus large-scale fluctuations) at $y^+ \approx 13$.

stresses:

$$\overline{u_i}|_{Cf_{LS}} = \int_{-\infty}^{+\infty}\int_{-\infty}^{+\infty}\int_{-\infty}^{+\infty} u_i \frac{P(u_1,u_2,u_3,Cf_{LS})}{P(Cf_{LS})} du_1 du_2 du_3 \qquad (1)$$

$$\begin{aligned}\overline{u_i'u_j'}|_{Cf_{LS}} &= \overline{(u_i-\overline{u_i}|_{Cf_{LS}})(u_j-\overline{u_j}|_{Cf_{LS}})}|_{Cf_{LS}} \\ &= \overline{u_iu_j}|_{Cf_{LS}} - \overline{u_i}|_{Cf_{LS}}\,\overline{u_j}|_{Cf_{LS}}\end{aligned} \qquad (2)$$

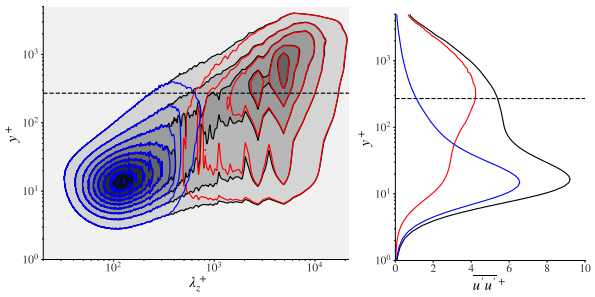

Figure 3. Large-scale/small-scale decomposed field of streamwise fluctuations; (a) Premultiplied power spectra: (black) total fluctuations, (red) large-scale fluctuations and (blue) remaining fluctuations; (b) corresponding streamwise-energy profiles.

Other properties, such as conditional production rates, follow likewise. The merit of these conditional values is that they bring to light the influence of large-scale fluctuations on the statistical quantities considered at large positive and negative Cf_{LS} values without the obscuring influence, or weighting, of low-density levels in the PDF $P(Cf_{LS})$, which is shown in Fig.4. The PDF is seen to be mildly positively skewed, a properly also observed at lower Reynolds number at which the level of skewness is markedly higher.

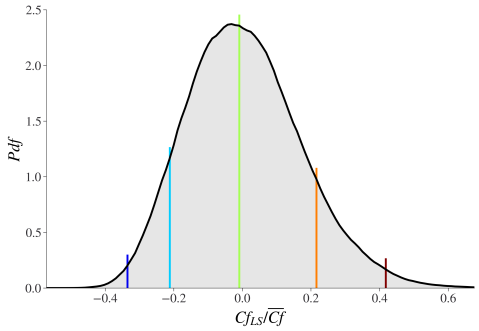

Figure 4. PDF of large-scale streamwise-velocity fluctuations derived from AE, dark blue and red lines correspond to 1% extreme events, light blue and orange lines correspond to 10% and green line to 50% (median of PDF).

2.3 Conditional analysis of length-scale modulation based on structure function

The second-order structure function is proposed herein as a basis for investigating length-scale modulation. Given the fields of velocity $u(x,z)$ across any y-plane, and the large-scale skin-friction $Cf_{LS}(x,z)$, the latter being wall footprint of the outer-large scale structures shifted forwards in streamwise direction by $\Delta x = \Delta y \tan\theta$, with $\theta \approx 11^o$, the starting point is the derivation of the PDFs from the DNS data set in which $s_{u,\delta z} = u(x,z+\delta z) - u(x,z)$ is the instantaneous difference between velocity fluctuations separated by a given (i.e. chosen) value δz (the subscript y is omitted henceforth).

The n^{th} order structure function (S^n) for a given δz can

be derived from:

$$S_u^n(\delta z) = \langle |u(x,z+\delta z) - u(x,z)|^n \rangle = \int s_{u,\delta z}^n P(s_{u,\delta z}) ds_{u,\delta z} \tag{3}$$

The representation of the structure function via its PDF is important in the context of, and is consistent with, the strategy of using the multi-variable joint PDF strategy, as expressed by equation (1).

Here, the focus is on the second-order structure function, or rather its incremental derivative with respect to δz, used as the surrogate of the scale-wise distribution of the energy. As demonstrated by Davidson *et al.* (2006*a*,*b*) and Agostini & Leschziner (2017) , there is a close relationship between the energy spectra and the derivative of the structure function. The preference for the structure function is rooted in the fact that it is a purely data-driven method, the results of which do not depend upon a projection basis and on how the hyper parameters are tuned, as is the case for FFT (window size, window function, etc.) and wavelet-based analyses (see De Moortel *et al.* (2004)). Moreover, as the conditional statistics are derived from the *joint pdf* of the structure function, the conditional wavelength can be determined without any specific constrains on the length of the input signal, as this latter can continuously vary with the value of Cf_{LS}. Another advantage of the structure function is that it allows the contribution of the largest scales resolved by the DNS to be represented much more accurately that via the spectra, which suffer from limitation imposed by the FFT when the sample of scales is sparse and the domain size limited. As will emerge below, length-scale shifts in this derivative will be used to identify length-scale modulation conditional on Cf_{LS}.

By using the multi-variable PDF approach, the variation of the structure function and its derivative conditional on Cf_{LS} can be investigated in the same sense as previously undertaken in relation to amplitude modulation, by way of:

$$S_u^n(\delta z) = \iint s_{u,\delta z}^n P(s_{u,\delta z}, Cf_{LS}) ds_{u,\delta z} dCf_{LS} \tag{4}$$

$$S_u^n(\delta z)|_{Cf_{LS}} = \int s_{u,\delta z}^n \frac{P(s_{u,\delta z}, Cf_{LS})}{P(Cf_{LS})} ds_{u,\delta z} \tag{5}$$

With the joint PDF, $P(s_{u,\delta z}, Cf_{LS})$, derived separately for each and every computational y place and for a set of values δz, the second-order structure function conditional on Cf_{LS} can be derived using equation (5) with $n = 2$. Alongside, the conditional structure function $S_u^2(\delta z)|_{Cf_{LS}}$, its premultiplied derivative $\delta z \frac{dS_u^2(\delta z)}{d\delta z}|_{Cf_{LS}}$ can be computed at every wall-normal location. It is this derivative on which attention focuses primarily. Again, the reason is that the variation of this variable across δz is closely connected to the energy-density spectrum $\Phi_{uu}(\lambda_z)$, with λ_z connected to the separation δz, as is discussed at length in Agostini & Leschziner (2017).

The objective here is to examine statistics that are conditional on a single reference field. This reference field is chosen to be Cf_{LS}. This allows questions to be asked about the validity of the quasi-steady concept which hypothesizes that scaling the wall-normal small-scale turbulence properties with the local large-scale wall shear stress $\tau_{w,LS}$ results in identical statistics, i.e. statistics that do not vary with Cf_{LS}. However, a question that needs to be addressed is whether the condition Cf_{LS} is equivalent to the condition $u_{LS}(y^+)$. This equivalence is substantially favoured by the fact that large-scale fluctuations are highly correlated in y^+, subject to a spatial streamwise lag, as is discussed by Hutchins & Marusic (2007) and several other authors. This has also been found to be the case in the present data set. Hence, here, the assumption has been invoked that u_{LS} is represented by Cf_{LS}, subject to the spatial lag $\Delta x^+ = \Delta y^+ \tan(\theta)$, with the angle arising from the two-point correlation maps. A consequence of this lag, and thus the gradient in u_{LS}, is a degree of ambiguity as regards the derivative of $S(\delta z)$, which is conditional of u_{LS} – or rather its Cf_{LS} equivalent. This is a problem similar to that discussed earlier in relation to spanwise variations in u_{LS}. However, the lag between two neighbouring y^+ planes is small and the effect on the statistics is thus negligible.

3 Amplitude modulation

Small-scale amplitude modulation by large-scale outer structures in wall-bounded flow has been studied extensively over the past decade or two, both experimentally and computationally, the latter by probing DNS data. Previous computational studies have been restricted to $Re_\tau < 1000$, in which case, the outer structures are relatively weak and the relevant interactions rather tenuous. Here, amplitude modulation is considered at the much higher Reynolds number $Re_\tau = 5200$.

An example is given in Fig.5(a,b), in which the conditional response of the streamwise stress to the large-scale skin friction Cf_{LS} is shown (the profiles are cuts at the Cf_{LS} shown in the Fig.5(a), corresponding values of $Cf_{LS}/\overline{Cf}$ are given in Fig.4). While this figure conveys a number of interesting features deserving discussion - not least the negative correlation between the outer large-scale fluctuations and the small-scale fluctuations in the outer region - the key feature to highlight here is that positive and negative footprints are associated, respectively, with strong positive modulation and damping. Fig.6 demonstrates that the modulation is driven by distortions in the conditional mean profiles, which then translate into corresponding variations in the stress-production rates, shown in Fig.7. Specifically, the production of the streamwise energy increases substantially at the wall for positive footprints and decreases for negative ones. The reverse occurs in the outer regions, although the strain increments are considerably weaker than in the inner layer, and this reversal ties up with the negative correlations between the stresses in the outer and inner regions, mentioned above by reference to Fig.5. These results illustrate the more general observation that the mechanisms by which the footprints provoke the modulation of near-wall turbulence within the near-wall layer concur broadly with those derived at the much lower Reynolds number at $Re_\tau = 1000$ presented by Agostini & Leschziner (2019*a*) .

The present processing methodology also allows light to be shed on the question of whether the turbulent stresses as well as production rates are universal when scaled with the local, instantaneous, large-scale wall shear stress – i.e., whether the Quasi-Steady Hypothesis (QSH) is satisfied (Chernyshenko (2021)). An example is shown in Fig.8, again by reference to the streamwise stress. When the streamwise stress and the wall-normal distance are normalised by the local large-scale shear stress, instead of its mean value (as in Fig.5), the wall-normal profiles of the conditional streamwise stress approximately collapse on one another, at least up to $y^+ \approx 80$. The implication is that the QSH is valid only in the region not much thicker than the buffer layer. The region well above the buffer layer is, in contrast, increasingly populated by intermediate-size structures with a lifetime longer

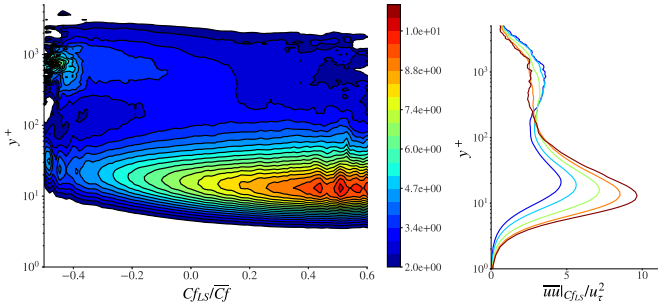

Figure 5. Conditional response of the streamwise stress to the large-scale skin friction Cf_{LS}, scaled with average u_τ. Profile colours correspond to locations in the pdf in Fig.4

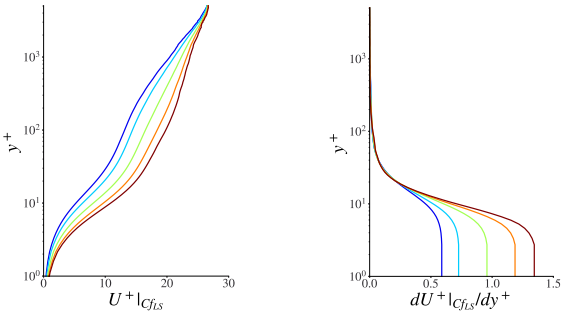

Figure 6. Profiles of conditional streamwise velocity and its wall-normal derivative at the locations marked in the pdf in Fig.4.

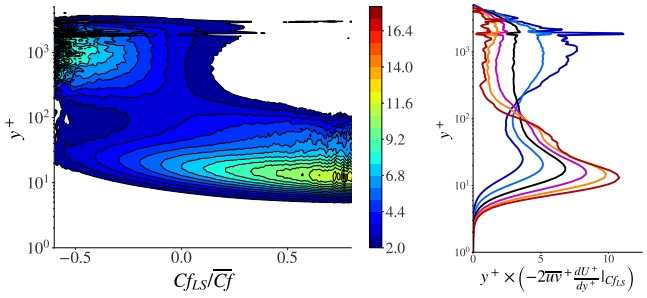

Figure 7. Conditional response of the production of the streamwise energy component to the large-scale skin friction, scaled with average u_τ. Profile colours correspond to locations in the pdf in Fig.4

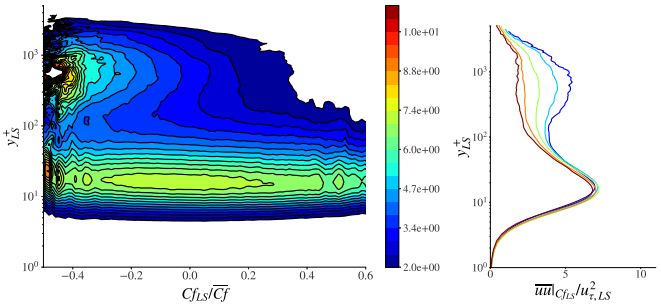

Figure 8. Conditional response of the streamwise stress to the large-scale skin friction Cf_{LS}, scaled with the local large-scale $u_{\tau,LS}$. Profile colours correspond to locations in the pdf in Fig.4

than the small-scale structures, and this detracts from applicability of the QSH. Consistently, the production rate for the streamwise stress, not included herein, also complies with the QSH in the near-wall region, but not beyond (a more extensive discussion of the pertinent mechanisms can be find in Agostini & Leschziner (2019*b*)).

4 Length-scale modulation

Fig.9 shows six maps of the premultiplied derivative of the second-order structure function in the $\delta z^+ - y^+$ plane at the six conditional values of Cf_{LS} shown in the pdf of figure 4. Attention is first drawn the choice of the abscissa: $4\delta z^+$. The choice of this multiplier is rooted in the correspondence between the derivative of the structure function and the spectra, an equivalence demonstrated and discussed in Agostini & Leschziner (2017). In the latter, the abscissa is conventionally the wave length λ_z^+. Multiplying δz^+ by 4 is observed to shift the peak in the map at $y^+ = 12$ and $Cf_{LS} = 0$ to the value to $4\delta z^+ \approx 100$, corresponding to $\lambda_z^+ \approx 100$ – i.e., the accepted level of the spanwise separation distance between streaks as derived from two-point correlations.

There are three observations that can now be made by reference to Fig.9 9. First, as Cf_{LS} increases, there is a progressive shift of the maximum towards the wall. This process and the mechanisms responsible have been discussed in detail in Agostini & Leschziner (2019*a*). In essence, large positive Cf_{LS} levels cause a steepening of the strain close to the wall, thus generating increased small-scale turbulence and thinning the viscous sublayer. More interesting in the present context is that the increase in Cf_{LS} is also accompanied by a progressive reduction in the length-scale maximum from $4\delta z^+ \approx 100$ to around 65, which may be interpreted as indicating the length-scale modulation. The third feature deserved to be highlighted is the progressive widening of the scale spectra around the buffer layer for increasing Cf_{LS}. This widening appears to be due primarily to a shift of the range of short length scales towards lower values, a process especially noticeable when tracking the left-most edge of the spectra at $y^+ \approx 10$. In contrast, the longer scales around the buffer layer, at $4\delta z^+ \approx 200$, experience no discernible shift (the downward-pointing tongues at $4\delta z^+ > 1000$ signify the footprinting process).

To examine whether the QSH applies to the length-scale modulation, a map of contours of the wave length corresponding to the maximum value of the derivative of the structure function at different y^+ values and conditional on Cf_{LS} is derived. This is shown in Fig.10(a). The map demonstrates that the wave length of the maximum derivative location at any given y^+ is decreasing, as already observed by reference to Fig.9. For example, at $y^+ \approx 13$, the wave length in Fig.10(a) is seen to decline from 100 (green shade) to around 70 (dark blue shade). Next, the map in Fig. 10(a) is re-scaled with the wall-normal distance and the wave length normalised with the large-scale wall shear stress and $\delta z^{+,LS} = \delta z^+ \times u_{\tau,LS}/u_\tau$. This yields the map given in Fig.10(b), which permits two major observations to be made. First, the contours are broadly horizontal in the positive range of Cf_{LS}, implying that the QSH applies to length-scale modulations of the fluctuations within the near-wall layer, $y^+ < 40$. Second, the hypothesis is not satisfied for negative large-scale fluctuations. As the length-scale modulation is here considered within the confines of the near-wall layer, up to y^+ of approximately 40, the lack of of adherence of length-scale fluctuations with the QSH at negative Cf_{LS} is inconsistent with the behaviour observed in respect

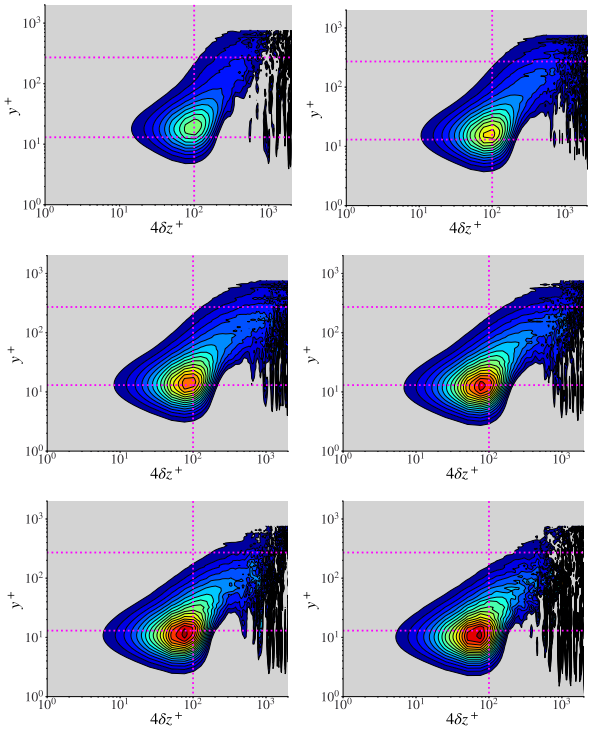

Figure 9. Maps of $\delta z \frac{dS_u^2(\delta z)}{d\delta z}|^+_{Cf_{LS}}$ in the $y^+ - \delta z^+$ plane conditional on the six Cf_{LS} shown in figure Fig.4; (a)-(f) arranged in order of rising Cf_{LS} values.

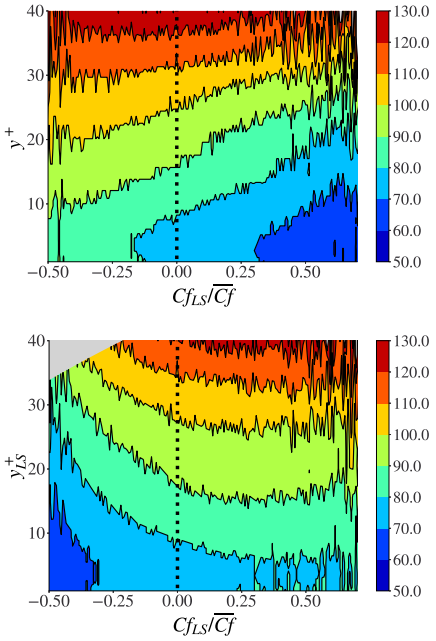

Figure 10. Maps of conditional $4\delta z^+|_{Cf_{LS}}$ in the $y^+ - Cf_{LS}$ plane derived from $\delta z \frac{dS_u^2(\delta z)}{d\delta z}|^+_{Cf_{LS}}$ (for streamwise fluctuations); (a) nominal field scaled with mean wall shear stress; (b) field in (a) rescaled with large-scale wall shear stress to demonstrate adherence to the quasi-steady hypothesis.

of the amplitude modulation. An interpretation of this inconsistency is given in a more extensive paper evolving at the time of writing.

REFERENCES

Agostini, L. 2020 Exploration and prediction of fluid dynamical systems using auto-encoder technology. *Physics of Fluids* **32** (6), 067103.

Agostini, L. & Leschziner, M. 2014 On the influence of outer large-scale structures on near-wall turbulence in channel flow. *Physics of Fluids* **26** (7), 075107.

Agostini, L. & Leschziner, M. 2017 Spectral analysis of near-wall turbulence in channel flow at $\mathrm{Re}_\tau = 4200$ with emphasis on the attached-eddy hypothesis. *Phys. Rev. Fluids* **2**, 014603.

Agostini, L. & Leschziner, M. 2019*a* The connection between the spectrum of turbulent scales and the skin-friction statistics in channel flow at $\mathrm{Re}_\tau \approx 1000$. *Journal of Fluid Mechanics* **871**, 22–51.

Agostini, L. & Leschziner, M. 2019*b* On the departure of near-wall turbulence from the quasi-steady state. *Journal of Fluid Mechanics* **871**.

Agostini, L. & Leschziner, M. 2021 Statistical analysis of outer large-scale/inner-layer interactions in channel flow subjected to oscillatory drag-reducing wall motion using a multiple-variable joint-probability-density function methodology. *Journal of Fluid Mechanics* **923**.

Chernyshenko, S. 2021 Extension of qsqh theory of scale interaction in near-wall turbulence to all velocity components. *Journal of Fluid Mechanics* **916**, A52.

Davidson, PA, Krogstad, P-A, Nickels, TB *et al.* 2006*a* A refined interpretation of the logarithmic structure function law in wall layer turbulence. *Physics of Fluids* **18** (6), 5112.

Davidson, PA, Nickels, TB & Krogstad, P-Å 2006*b* The logarithmic structure function law in wall-layer turbulence. *Journal of Fluid Mechanics* **550**, 51 –60.

De Moortel, I., Munday, SA & Hood, A.W. 2004 Wavelet analysis: the effect of varying basic wavelet parameters. *Solar Physics* **222** (2), 203–228.

Guastoni, L., Güemes, A., Ianiro, A., Discetti, S., Schlatter, Ph., Azizpour, H. & Vinuesa, R. 2021 Convolutional-network models to predict wall-bounded turbulence from wall quantities. *Journal of Fluid Mechanics* **928**.

Hutchins, N. & Marusic, I. 2007 Large-scale influences in near-wall turbulence. *Philosophical Transactions of the Royal Society of London A: Mathematical, Physical and Engineering Sciences* **365** (1852), 647–664.

Lee, M. & Moser, R. D. 2015 Direct numerical simulation of turbulent channel flow up to $\mathrm{Re}_\tau \approx 5200$. *Journal of Fluid Mechanics* **774**, 395 –415.

Touber, E. & Leschziner, M. A. 2012 Near-wall streak modification by spanwise oscillatory wall motion and drag-reduction mechanisms. *Journal of Fluid Mechanics* **693**, 150 –200.

Vincent, Pascal, Larochelle, Hugo, Lajoie, Isabelle, Bengio, Yoshua, Manzagol, Pierre-Antoine & Bottou, Léon 2010 Stacked denoising autoencoders: Learning useful representations in a deep network with a local denoising criterion. *Journal of machine learning research* **11** (12).

Zhou, Chong & Paffenroth, Randy C 2017 Anomaly detection with robust deep autoencoders. In *Proceedings of the 23rd ACM SIGKDD international conference on knowledge discovery and data mining*, pp. 665–674.